Available online at www.sciencedirect.com
ScienceDirect
Trans. Nonferrous Met. Soc. China 21(2011) 2617−2625
Transactions of Nonferrous Metals Society of China
www.tnmsc.cn

Hot corrosion behavior of Ni–16Cr–*x*Al based alloys in mixture of Na_2SO_4−NaCl at 600 °C

LI Wei-jie[1], LIU Yong[1], WANG Yan[1], HAN Chao[1], TANG Hui-ping[2]

1. State Key Laboratory of Powder Metallurgy, Central South University, Changsha 410083, China;
2. State Key Laboratory of Porous Metals Materials, Northwest Institute for Nonferrous Metal Research, Xi'an 710016, China

Received 11 April 2011; accepted 7 September 2011

Abstract: The hot corrosion behaviors of Ni–16Cr–*x*Al(*x*=4.5%, 6.8%, 9.0%, mass fraction) based alloys in Na_2SO_4–25% NaCl molten salts at 600 °C were investigated. The effects of pre-oxidation and Al content on the resistance to hot corrosion were examined. The hot corrosion resistance of Ni–16Cr–*x*Al based alloy with Al addition from 4.5% to 9.0% increases with increasing Al content. The alloy with Al content of 9.0% shows the highest hot corrosion resistance among the examined alloys because more *β*–NiAl phases are obtained to sustain the Al_2O_3 scale repaired during hot corrosion. Pre-oxidized specimens have a superior hot corrosion resistance compared with the as-cast specimens, due to a protective oxide scale formed after pre-treatment.
Key words: Ni–16Cr–*x*Al based alloys; pre-oxidation; Na_2SO_4–25% NaCl mixed salt; hot-corrosion mechanism

1 Introduction

The energy crisis and protection of the environment require that coal-fired power plants have high power and low emissions, which introduces new demands for filter materials, such as hot corrosion resistance and good high-temperature mechanical properties [1−3]. Although the metallic filters based on the Fe_3Al intermetallic compound have been well developed, the brittle properties at ambient temperature and insufficient high temperature strength make it difficult to withstand typical operating conditions. Recently, Ni–Cr–Al based alloy has attracted much attention in the field of gas purification at high temperature, because of its both nearly equivalent resistance to high temperature corrosion as the Fe_3Al and good mechanical properties [4]. However, investigations about the hot corrosion behavior of Ni–Cr–Al based alloys were still limited [5−6].

For the Ni−Cr alloys, there are some reports about the effect of Al addition from 0 to 6% on its sulfidation behavior [7−8]. MOTOI and YUTAKA [7] studied the corrosion behaviors of Ni–20Cr, Ni–20Cr–2Al and Ni−20Cr−5Al alloys immersed in molten Na_2SO_4–NaCl at 1 173 K. The corrosion mass loss was found to increase with the increase of the Al content. However, researches on Ni−Cr−*x*Al (*x*=1%, 3%, 4.5%, 6%) alloys tested in a burner rig with diesel fuel burned at 870 °C showed that a peak of corrosion mass loss appeared in the Ni–Cr alloy with 4.5% Al. Whereas, there existed a smaller value of the corrosion mass loss for Ni–Cr alloy with 6% Al compared with the Ni–Cr alloy with 4.5% Al [8]. Therefore, it was deduced that the sulfidation resistance of the Ni–Cr alloys, with Al content larger than 4.5%, increased with increasing Al content.

In the present study, the hot corrosion behaviors of Ni–16Cr–*x*Al based alloys with 4.5%, 6.8% and 9.0% Al in Na_2SO_4–25% NaCl molten salts at 600 °C were examined. The effect of pre-oxidation on the hot corrosion behaviors of the Ni–16Cr–*x*Al based alloys with different contents of aluminum was studied. The corroded scales were systematically characterized. Furthermore, the mechanism was discussed and possible sulfidation process of the pre-oxidized alloys was proposed.

Foundation item: Project (2009AA032601) supported by the National High-tech Research and Development Program of China
Corresponding author: LIU Yong; Tel: +86-731-88830406; E-mail: yonliu11@yahoo.com.cn
DOI: 10.1016/S1003-6326(11)61100-X

2 Experimental

Three Ni–16Cr–*x*Al based alloys containing different aluminum contents of 4.5%, 6.8% and 9.0% were prepared using high-purity materials (99.99%) by arc melting in a vacuum furnace. The nominal compositions of the alloys are shown in Table 1. The as-cast alloys were cut into cylindrical specimens of 8 mm in diameter and 7 mm in height. The surfaces of the specimens were polished with SiC papers down to 2000 grit, cleaned sequentially in alcohol and distilled water in an ultrasonic bath, and then dried in hot air. Pre-oxidation treatment was conducted in the mixture of nitrogen (with the flow rate of 0.03 m^3/h) and air at 1 000 °C for 50 h, followed by air cooling. The as-cast and pre-oxidized specimens were then put into the Al_2O_3 crucibles, immersed completely in the mixed Na_2SO_4–25%NaCl salts, and placed in a tube resistance furnace. The corrosion tests were conducted at 600 °C in air for 25, 50, 75, and 100 h, respectively. After the tests, the samples were washed with boiling distilled water to dissolve the remains of Na_2SO_4–NaCl, and to remove the loose corrosion products with hydrochloric acid. The morphology and compositions of the surface for the corroded specimens were investigated by field emission scanning electron microscope (FE-SEM, Nova Nanosem 230) equipped with an energy dispersive spectroscope (EDS). The phase compositions of the corroded scales were determined by X-ray diffraction (XRD, Rigaku, D/max−2550VB). Both of the specimens before and after corrosion tests were measured using an electronic balance with an accuracy of 0.1 mg.

Table 1 Nominal compositions of studied alloys

Alloy	*w*(Cr)/%	*w*(Al)/%	*w*(Fe)/%	*w*(C)/%	*w*(Y)/%
Ni−16Cr−4.5Al	16	4.5	3.0	0.05	0.01
Ni−16Cr−6.8Al	16	6.8	3.0	0.05	0.01
Ni−16Cr−9.0Al	16	9.0	3.0	0.05	0.01

Alloy	*w*(Mn)/	*w*(Si)/%	*w*(Zr)/%	*w*(B)/%	*w*(Ni)/%
Ni−16Cr−4.5Al	0.5	0.2	0.1	0.01	Bal.
Ni−16Cr−6.8Al	0.5	0.2	0.1	0.01	Bal.
Ni−16Cr−9.0Al	0.5	0.2	0.1	0.01	Bal.

3 Results

3.1 Kinetics of hot corrosion

Figure 1 shows the mass change per unit area of the pre-oxidized and as-cast specimens as a function of time in the Na_2SO_4–25% NaCl molten salts at 600 °C. It can be seen that the mass loss of the alloys increases with the exposure time extending. For the as-cast alloys, the mass loss decreases with the increment of aluminum content, and the Ni–16Cr–9.0Al alloy has the lowest mass loss of 5.97 mg/cm^2 after hot corrosion for 100 h. For the pre-oxidized samples, the mass change versus time curves exhibits relatively stable. Besides, the mass losses of the pre-oxidized samples are obviously lower than that of the as-cast alloys, as seen from Fig. 1. The pre-oxidized Ni–16Cr–9.0Al alloy has the lowest mass loss (0.75 mg/cm^2) after exposure for 100 h, which is about 12.6% of the mass loss for the corresponding as-cast alloy. According to the results above, it is concluded that both the pre-oxidation treatment and increasing the aluminum content can improve the hot corrosion resistance of Ni–16Cr–*x*Al alloys in the mixture of Na_2SO_4–25% NaCl salts at 600 °C to a certain extent.

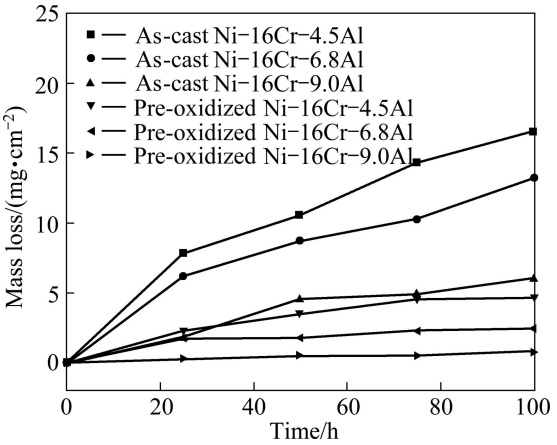

Fig. 1 Mass change per unit area of pre-oxidized and as-cast specimens as function of time in Na_2SO_4–25% NaCl salts at 600 °C

3.2 Corrosion products

Figure 2 shows the XRD patterns of the as-cast and pre-oxidized Ni–16Cr–*x*Al alloys before and after hot corrosion for 100 h at 600 °C. *β*–NiAl phase is detected on the surfaces of the as-cast Ni–16Cr–6.8Al and Ni–16Cr–9.0Al alloys (Fig. 2(a)). Meanwhile, both the amount and intensity of *β*–NiAl characteristic peak increase with increasing the Al content. Cr_2O_3, Al_2O_3 and Ni_3S_2 are the common oxide phases in the corroded scales of the as-cast alloys after hot corrosion (Fig. 2(a)). In addition, a small amount of NiO is also observed on the surface of Ni–16Cr–4.5Al alloy. Compared with the Ni–16Cr–4.5Al alloy, both of the amount and intensity of Al_2O_3 characteristic peaks on the surfaces of Ni–16Cr–6.8Al alloy and Ni–16Cr–9.0Al alloy increase, as seen from Fig. 2(a), due to the increment of aluminum content. After pre-treatment, oxide layers form on the surfaces of the Ni–16Cr–*x*Al alloys. The main phases of the products on the surface of pre-oxidized Ni–16Cr–4.5Al alloy are Al_2O_3 and Cr_2O_3. Meanwhile, a

small amount of $NiCrO_4$ is also observed (Fig. 2(b)). However, there is only Al_2O_3 identified on the surfaces of pre-oxidized Ni–16Cr–6.8Al alloy and Ni–16Cr–9.0Al alloy. After exposure for 100 h in the Na_2SO_4–25% NaCl molten salts at 600 °C, a trace amount of NiO and Ni_3S_2 are also found on the surfaces of pre-oxidized samples, as seen from Fig. 2(b).

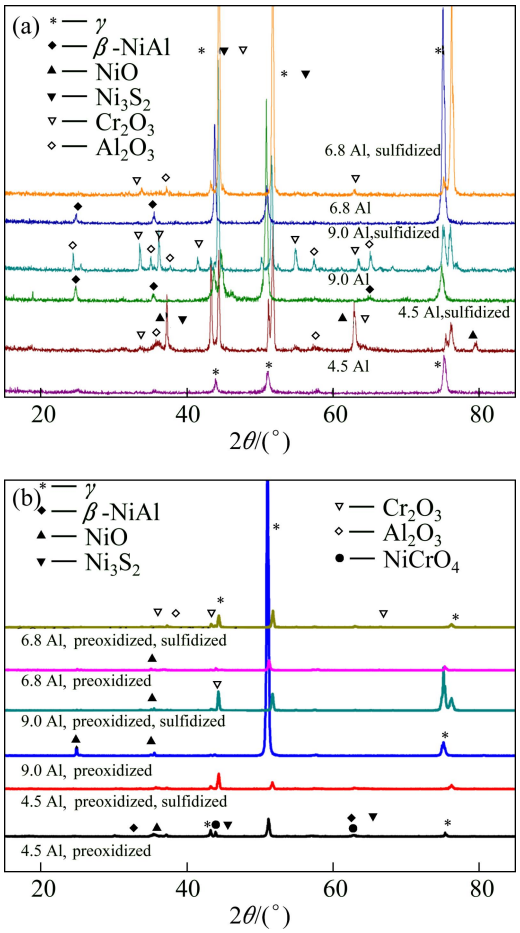

Fig. 2 XRD patterns of as-cast (a) and pre-oxidized (b) Ni–16Cr–*x*Al alloys before and after hot corrosion for 100 h at 600 °C

3.3 SEM (EDS) analysis of scale

The cross-sectional morphologies of the pre-oxidized Ni–16Cr–*x*Al alloys are presented in Fig. 3. It can be seen that relatively continuous and compact layers are formed on the surfaces of the pre-oxidized samples. The average thickness of the oxide layer on the Ni–16Cr–4.5Al alloy after pre-oxidation is about 4.5 μm (Fig. 3(a)), which is rich in O, Cr and Al as determined by EDS analysis. Combining the results of XRD and EDS, it can be deduced that the oxide phases are mainly Cr_2O_3 and partially Al_2O_3. Figure 3(b) shows the cross-section of the pre-oxidized Ni–16Cr–6.8Al alloy, and the scale with a thickness of 2.8 μm is thinner than that of the pre-oxidized Ni–16Cr–4.5Al alloy. The oxide scale formed on the surface of the pre-oxidized Ni–16Cr–9.0Al alloy is more uniform and compact, as seen from Fig. 3(c), with a thickness of 2.8 μm. The EDS analysis shows that the oxide scales of the pre-oxidized Ni–16Cr–6.8Al and pre-oxidized Ni–16Cr–9.0Al alloys are composed of Al_2O_3.

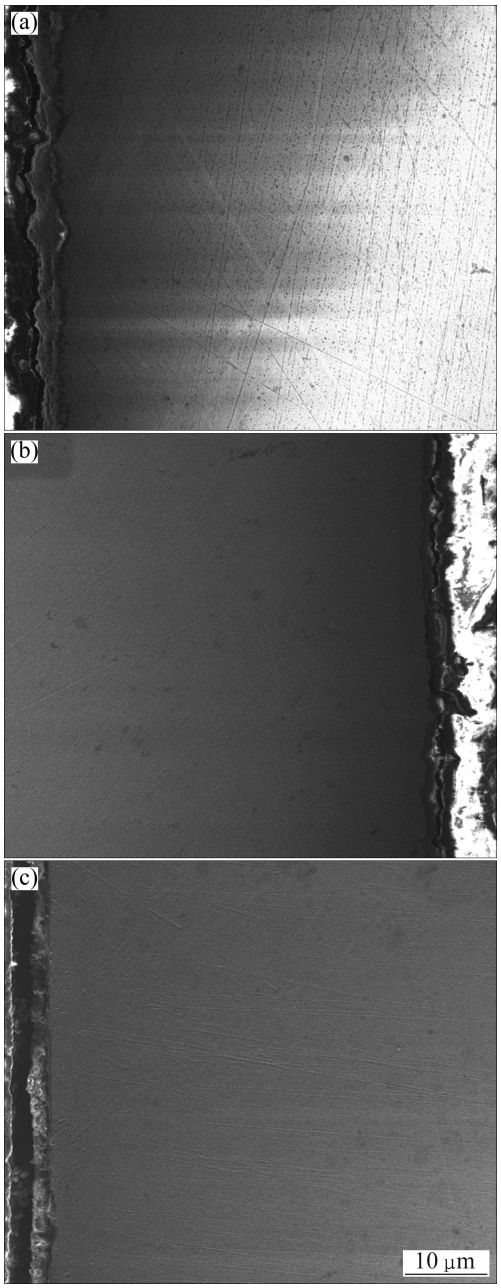

Fig. 3 Cross-sectional morphologies of pre-oxidized Ni–16Cr–*x*Al alloys: (a) Ni–16Cr–4.5Al alloy; (b) Ni–16Cr– 6.8Al alloy; (c) Ni–16Cr–9.0Al alloy

Figure 4 shows the cross-section of the as-cast samples and pre-oxidized samples corroded for 100 h in the Na_2SO_4–25% NaCl molten salts at 600 °C. It is revealed that a relatively thick corrosion layer forms on the surface of as-cast Ni–16Cr–*x*Al alloys, and a rather deep corrosion affected zone appears beneath the corrosion layer (Figs. 4(a)–(c)). However, the corrosion

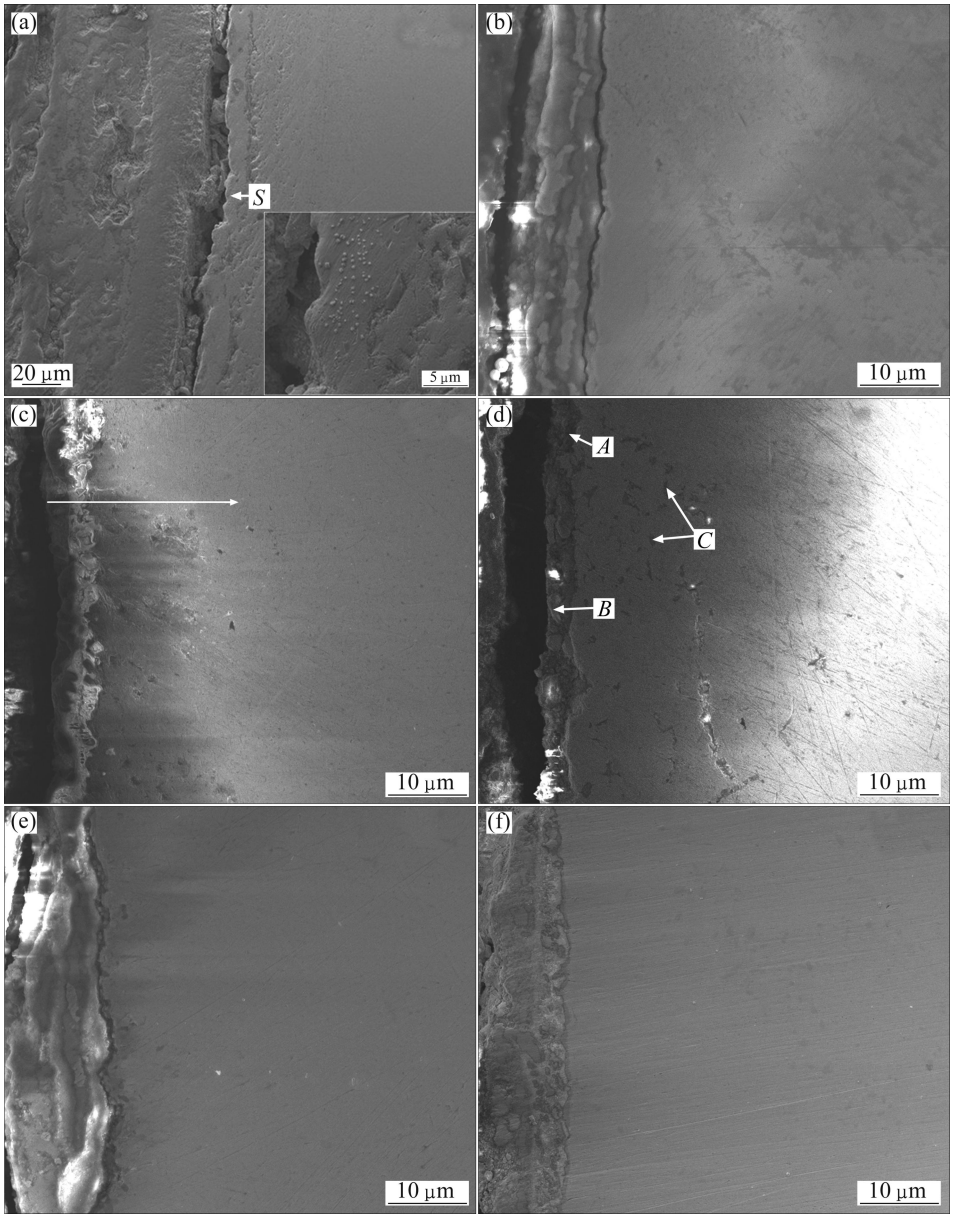

Fig. 4 Cross-sections of as-cast samples (a, b and c) and pre-oxidized samples (d, e and f) corroded for 100 h in Na_2SO_4–25% NaCl salts at 600 °C: (a), (b), (c) As-cast alloys with Al contents of 4.5%, 6.8%, 9.0%, respectively; (d), (e), (f) Pre-oxidized alloys with Al contents of 4.5%, 6.8%, 9.0%, respectively

affected zone is not observed beneath the corrosion layers of the pre-oxidized samples except for Ni–16Cr–4.5Al alloy (Figs. 4(d), (e)). The results above are consistent with those of the corrosion kinetics analysis in Section 3.1. That is, the hot corrosion resistance of the pre-oxidized samples is superior to that of the as-cast samples. As seen from Fig. 1 and Fig. 4, the hot corrosion resistance of the pre-oxidized Ni–16Cr–4.5Al alloy was comparable with that of the as-cast Ni–16Cr–9.0Al alloy.

It is evident that the as-cast Ni–16Cr–4.5Al alloy suffers serious hot corrosion, with a thickness of corrosion scale about 100 μm (Fig. 4(a)). A higher magnification of the region marked *S* in Fig. 4(a) shows that there are many small white grains and strip-like dark gray pits in it. The EDS analysis exhibits that the small white grains mainly contain Ni and S, while the strip-like dark gray pits are mainly composed of Ni and O. Figure 5 shows the element distribution map of the as-cast Ni–16Cr–4.5Al after corrosion for 100 h. It may be clearly noted that the corroded scale is mainly rich in Cr, Al and O, besides, there is also a small amount of S and Ni. Meanwhile, Al-depleted and Cr-depleted zones are detected beneath the corroded scale (Fig. 5), due to the outward diffusion of Al and Cr. In combination of XRD with EDS results, the corroded products in the scale of the as-cast Ni–16Cr–4.5Al alloy are Al_2O_3, Cr_2O_3, Ni_3S_2 and NiO.

As shown in Fig. 4(b), the corroded scale formed on the as-cast Ni–16Cr–6.8Al alloy is thinner than that on the as-cast Ni–16Cr–4.5Al alloy (Fig. 4(a)), with a thickness of 10 μm. Figure 6 shows the element distribution map of the cross-section. For the as-cast Ni–16Cr–6.8Al alloy, the compositions of the corroded scale are found to be similar to the results of the as-cast Ni–16Cr–4.5Al alloy, i.e., Cr, Al and O with a small amount of Ni and S.

It can be seen from Fig. 4(c) that after hot corrosion for 100 h, a thinner corroded scale with a thickness of 6 μm and deeper corrosion affected zone of about 18 μm beneath the scale are observed on the cross-section of as-cast Ni–16Cr–9.0Al alloy. Figure 7 shows the line

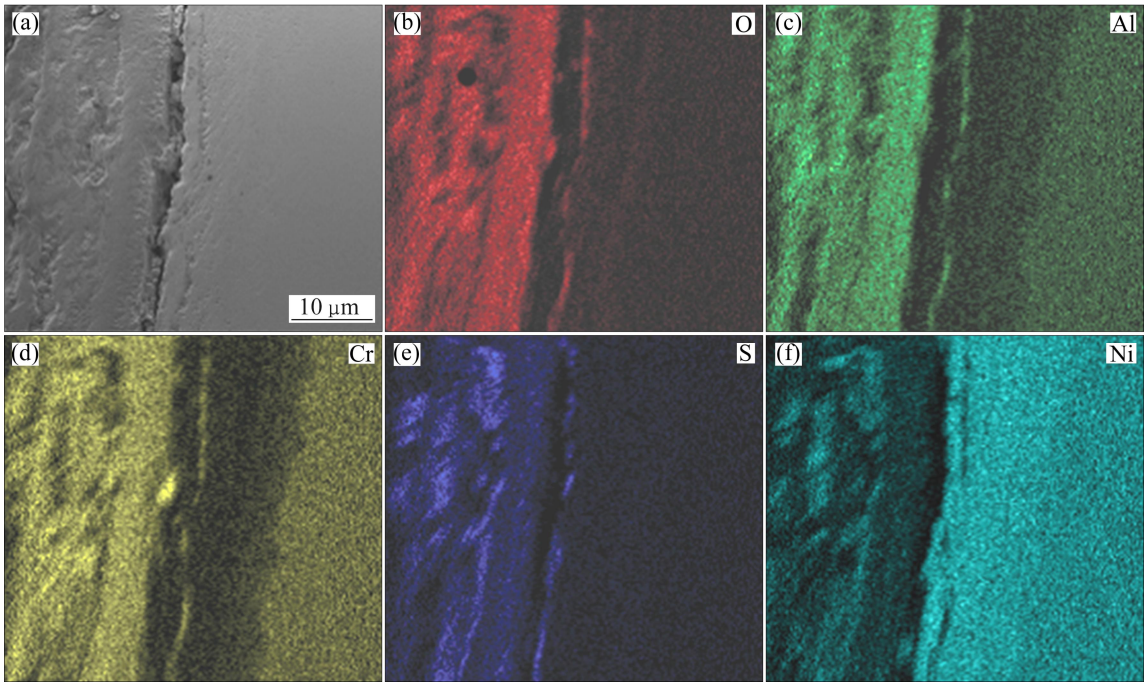

Fig. 5 Cross-sectional SEM image (a) and corresponding elements mapping (b, c, d, e, f) of as-cast Ni–16Cr–4.5Al after corrosion for 100 h in Na_2SO_4–25% NaCl at 600 °C

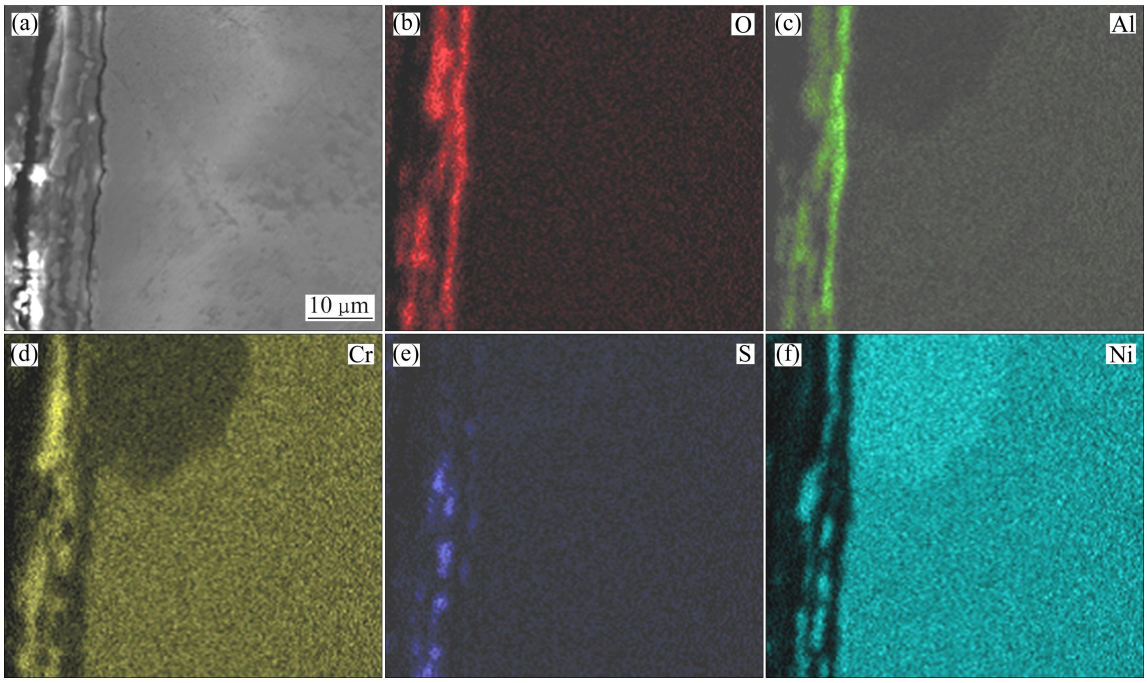

Fig. 6 Cross-sectional SEM image (a) and corresponding elements mapping (b, c, d, e, f) of as-cast Ni–16Cr–6.8Al after corrosion for 100 h in Na_2SO_4–25% NaCl at 600 °C

distribution of different elements along the arrow marked in Fig. 4(c). It is clearly found that two layers constitute the corroded scale, including an outer Cr_2O_3 layer and inner Al_2O_3 layer. A trace amount of sulfur is determined in the corrosion affected zone, which implies that the internal sulfidation occurs in the region.

For the pre-oxidized Ni–16Cr–4.5Al alloy, the corroded scale is about 3 μm and the corrosion affected zone is about 15 μm beneath the scale after being corroded for 100 h (Fig. 4(d)). The EDS results reveal that the continuous dark phase (marked as *A* in Fig. 4(d)) in the corrosion products mainly consists of Cr and O,

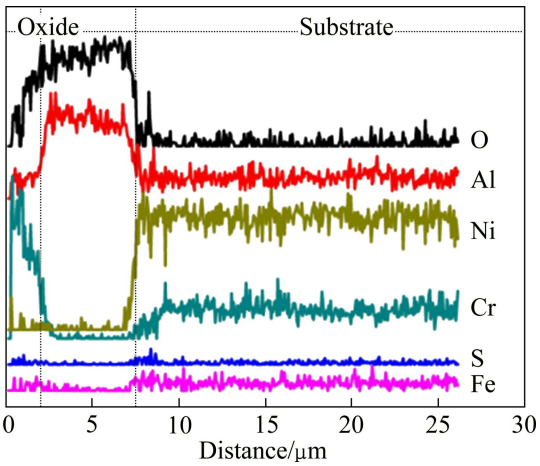

Fig. 7 Element distribution along arrow marked in Fig. 4(c) after corrosion for 100 h in Na_2SO_4–25% NaCl at 600 °C

and the slight gray phase (marked as *B* in Fig. 4(d)) is primarily composed of Al, O and Cr. Whereas, the corrosion affected zone (marked as *C* in Fig. 4(d)) is rich in O. By combining the results of XRD and EDS, it is deduced that the continuous dark phase and slight gray phase are Cr_2O_3 and Al_2O_3, respectively.

Figures 4(e) and (f) show the morphologies of the pre-oxidized Ni–16Cr–6.8Al and Ni–16Cr–9.0Al alloys after hot corrosion at 600 °C for 100 h, respectively. A corroded layer with a thickness of about 10 μm is observed, but the corrosion affected zone can be hardly found. The corresponding element distribution maps of the cross-sections are presented in Fig. 8 and Fig. 9, respectively. It may be noted from Fig. 8 that the corroded scale formed on the pre-oxidized Ni–16Cr–6.8Al alloy is mainly rich in Cr, Al, O and S, with a small amount of Ni. Combined with the chemical composition analysis of the pre-oxidized samples, the Al_2O_3 scale, which was formed during pre-oxidation, effectively retards the inward diffusion of sulfur to alloy/scale interface. Therefore, the sulfide was mainly distributed in the outer oxidized scale rather than substrate. The chemical composition of the corroded scale for the pre-oxidized Ni–16Cr–9.0Al alloy, as seen from Fig. 9, is similar to that of the pre-oxidized Ni–16Cr–6.8Al alloy. However, the scale formed on the pre-oxidized Ni–16Cr–9.0Al alloy is more compact, continuous and uniform in comparison with that of the pre-oxidized Ni–16Cr–6.8Al alloy.

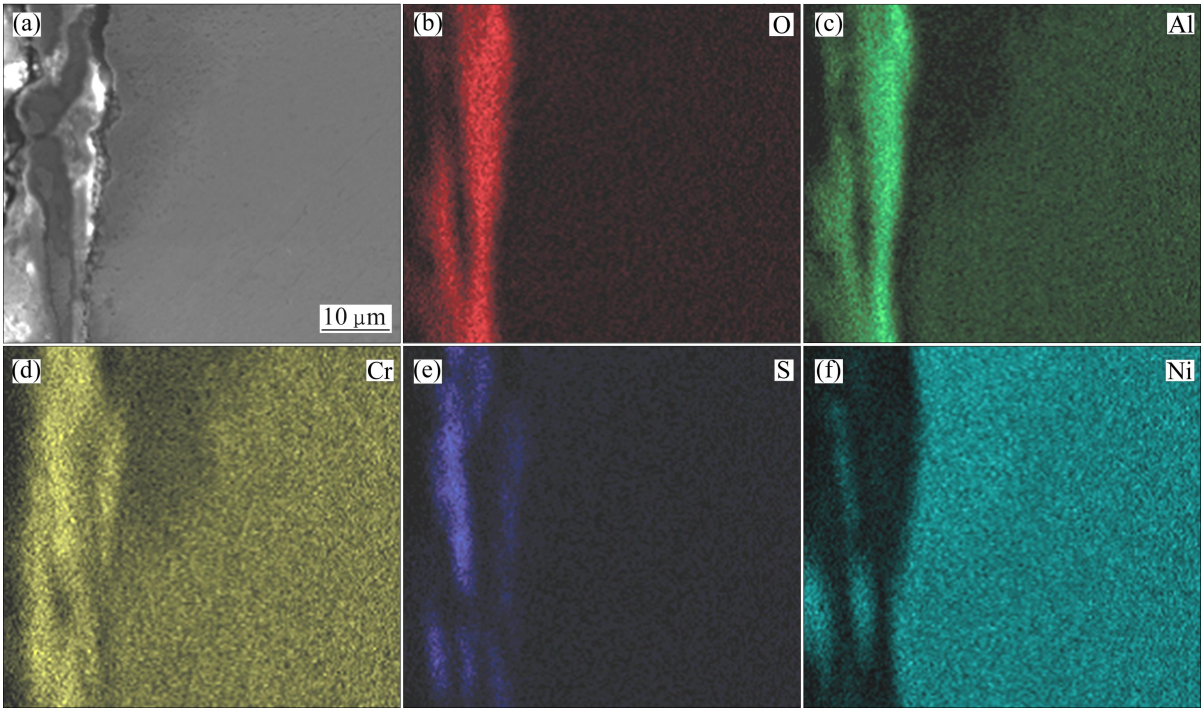

Fig. 8 Cross-sectional SEM image (a) and corresponding elements mapping (b, c, d, e, f) of pre-oxidized Ni–16Cr–6.8Al after corrosion for 100 h in Na_2SO_4–25% NaCl at 600 °C

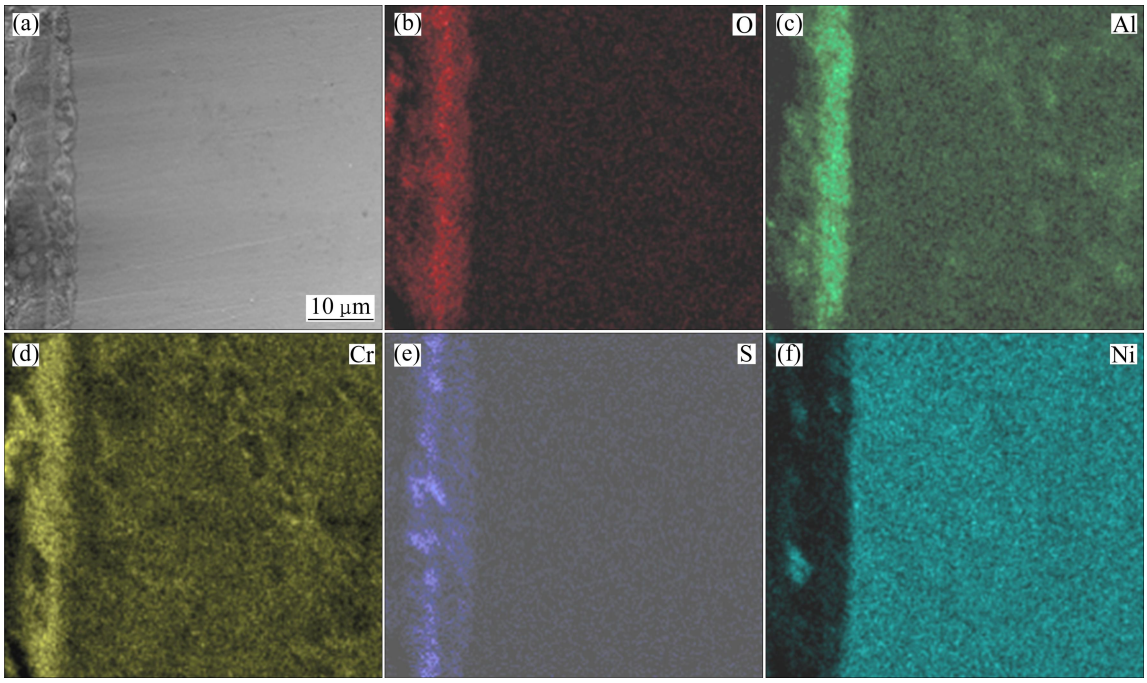

Fig. 9 Cross-sectional SEM image (a) and corresponding elements mapping (b, c, d, e, f) of pre-oxidized Ni–16Cr–9.0Al after corrosion for 100 h in Na_2SO_4–25% NaCl at 600 °C

4 Discussion

4.1 Hot corrosion mechanism

When immersed in the mixed salts, the as-cast samples were oxidized firstly by the dissolved oxygen [9]. Alumina and chrome were formed according to the selective oxidation, and the mixed salts would easily react with the oxides. Under this condition, the oxides could hardly form continuous protective oxide layer and thus serious hot corrosion occurred. According to the reaction $2SO_4^{2-}=2O^{2-}+3O_2+2S$ [10−11], it was known that the continuous formation of the oxides on the surface of the alloy lowered the $p(O)_2$ in the salts and increased the sulphur potential, leading to the transport through the oxide scale and the formation of sulfide at the interface of scale and metal. As seen from Fig. 5 and Fig. 6, sulfides are detected at the interface of scale and metal. It was suggested that $NiSO_4$ was formed by outward diffusion of Ni through the sulfide, and the reaction [12] $9Ni+2NiSO_4=8NiO+Ni_3S_2$ subsequentially took place, which can explain the production of NiO and Ni_3S_2 (Fig. 2(a)).

The oxide scale formed during the oxidation stage, had a certain effect on inhibiting the invasion of sulfur. However, the forming sulfide caused a reduction of S activity and consequently an increase of O^{2-} activity at the interface, which finally initiated basic fluxing of the oxide scale. Moreover, Cr_2O_3 is more stable than Al_2O_3 in Na_2SO_4 since it disobeys the Rapp-Goto's criterion of negative solubility gradient for self sustained dissolution [13]. The basic dissolution of Al_2O_3 took place as $Al_2O_3+2O_2=2\,AlO_2^-$. Therefore, more Al was required to diffuse outward from the substrate to reform the Al_2O_3 scale. This implied that there was a competition between the destructive dissolution and the re-formation of Al_2O_3 scale. It has been reported that the β-NiAl phase could act as an Al-reservoir [14−17]. Consequently, the β-NiAl phase beneath the alloy surface could provide the Al to repair the Al_2O_3 scale. With time extending, the β-NiAl phase existing inside the substrate was hardly found due to the heavy consumption of aluminum (Fig. 2(a)). There was not sufficient β-NiAl phase for the as-cast Ni–16Cr–xAl alloys to sustain the scale repaired. However, with the increment of the Al content, more β-NiAl phases are detected in the Ni–16Cr–xAl alloys (Fig. 2(a)). Thus, for Ni–16Cr– 9.0Al alloy, more Al could be accommodated and supplied to form the alumina scale. As a result, a uniform and compact Al_2O_3-rich scale formed on the surface of Ni–16Cr–9.0Al alloy (Fig. 7), which was able to act as an effective protective barrier between the substrate and the salts medium. Therefore, the Ni–16Cr–9.0Al alloy exhibited a better resistance to the hot oxidation than the other two Ni–16Cr–xAl alloys.

4.2 Effect of pre-oxidation on hot corrosion

The pre-oxidized Ni–16Cr–xAl alloys exhibit much better hot corrosion resistance than the as-cast alloys in Na_2SO_4–25%NaCl at 600 °C for 100 h (Fig. 1). The

pre-oxidized layers are found to still exist on the surfaces of specimens after hot corrosion (Figs. 4(e), (f)). Moreover, it is noted that for the pre-oxidized samples except for the Ni–16Cr–4.5Al alloy sulfur is not detected in the substrate after hot corrosion (Fig. 8 and Fig. 9). This may be ascribed to the fact that the continuous, compact and protective oxide layer formed during pre-oxidation could effectively inhibit the inward diffusion of sulfur. The sulfidation process of the pre-oxidized alloys could be considered to follow a sequence presented in Fig. 10. Firstly, Ni^{2+}, Cr^{3+} and Al^{3+} diffuse outward and S^{2-} inward through the oxide layer, as shown in Fig. 10(a). Then, sulfides nucleate at the oxide/salt interface, leading to the formation of a sulfide layer (Fig. 10(b)). With time going on, the S^{2-} ions diffuse through the oxide layer and the cations diffuse outward, resulting in the formation of the sulfides within the oxide layer (Fig. 10(c)). With continued exposure to the sulfidizing environment, more S^{2-} ions diffuse through the oxide layer and sulfide growth takes place at the oxide/metal interface, as shown in Fig. 10(d). Accordingly, for the pre-oxidized samples, the ability of the preformed oxide scale to inhibit the diffusion of sulfur is a key factor in the hot corrosion resistance.

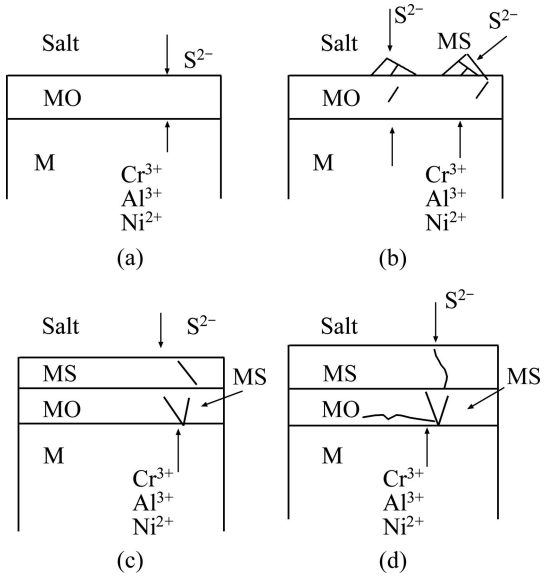

Fig. 10 Schematic diagram showing growth of sulfide layer on pre-oxidized Ni–16Cr–*x*Al alloys during hot corrosion in Na_2SO_4–25% NaCl at 600 °C: (a) Diffusion of S^{2-}, Al^{3+}, Cr^{3+} and Ni^{2+} in oxide layer; (b) Nucleation of sulfides at oxide/salt interface; (c) Formation of sulfides in oxide layer; (d) Growth of sulfides near oxide/alloy interface

The pre-oxidized Ni–16Cr–6.8Al and Ni–16Cr–9.0Al alloys have a superior hot corrosion resistance than the pre-oxidized Ni–16Cr–4.5Al alloy (Fig. 1). The preformed scale formed on the Ni–16Cr–4.5Al alloy is mainly Cr_2O_3 and partially Al_2O_3, while that on the Ni–16Cr–6.8Al alloy and Ni–16Cr–9.0Al alloy are Al_2O_3 (Fig. 3). A distinct difference existed between chromia and alumina films with respect to their abilities to inhibit sulfidation. The diffusivity of sulfur in Cr_2O_3 was 3.6×10^{-10} cm^2/s at 1 000 °C, while in Al_2O_3 was 7.9×10^{-13} cm^2/s at 1 000 °C [18]. The time for sulfur penetrating the scales at 600 °C can be approximately calculated using the diffusivity of sulfur at 1 000 °C. It was shown that the time required for sulfur to penetrate a 4.5 μm-thick film of Cr_2O_3 (Fig. 3(a)) at 600 °C was less than 10 min; however, for sulfur to penetrate an Al_2O_3 scale with a thickness of 2.8 μm (Figs. 3(b), (c)) at 600 °C it took about 28 h. Therefore, it can be concluded that the alumina films are an inherently good barrier to sulfidation in comparison with chromia films.

5 Conclusions

1) The hot corrosion resistance of Ni–16Cr–*x*Al alloy, with 4.5%–9.0% Al in the Na_2SO_4–25%NaCl salts at 600 °C, increases with the increasing Al content. The hot corrosion resistance of the alloys can be improved by pre-oxidation treatment.

2) A relatively continuous, compact and protective oxide scale is formed on the surface of pre-oxidized Ni–16Cr–*x*Al alloys. The oxide scale consisting of Cr_2O_3 and partially Al_2O_3 is formed on the surface of pre-oxidized Ni–16Cr–4.5Al alloy, while a protective oxide scale only containing Al_2O_3 is formed on the surfaces of the pre-oxidized Ni–16Cr–6.8Al and Ni–16Cr–9.0Al alloys. Alumina films are suggested to be inherently good barriers to sulfidation in comparison with chromia films.

References

[1] PEUKERT W. High temperature filtration in the process industry [J]. Filtration & Separation, 1998, 35: 461−464.

[2] ERIKSSON T, ISAKSSON J, STAHLBERG P, KURKELA E, HELANTI V. Durability of ceramic filters in hot gas filtration [J]. Bioresource Technology, 1993, 46: 103−112.

[3] LUCKE T, FISSAN H. The prediction of filtration performance of high efficiency gas filter elements [J]. Chemical Engineering Science, 1996, 51: 1199−1208 .

[4] TERPSTRA R L, ANDERSON I E, GLEESON B. Development of metallic hot gas filters [C]//2001 International Conference on Powder Metallurgy and Particulate Materials. New Orleans, USA: Metal Powder Industries Federation, 2001: 84−97.

[5] El-DAHSHAN M E, WHTTEL D P, STRINGER J. Hot corrosion of nickel-based alloys containing aluminium and molybdenum [J]. Materials and Corrosion, 1974, 25 (12): 910−916 .

[6] HARA M, OKUMURA H, NAKAGAWA T, SATO Y, SHINATA Y. Effect of pre-oxidation on hot corrosion of Ni-Cr-Al alloy in molten Na_2SO_4-NaCl [J]. Journal of the Japan Institute of Metals, 1995, 59: 1259−1265.

[7] MOTOI H, YUTAKA S. Electrochemical studies on hot corrosion of Ni−Cr−Al alloys in molten Na_2SO_4-NaCl [J]. Materials Transactions,

JIM, 1992, 33(8): 758−765.
[8] MORROW H, SPONSELLER D L, KALNS E. The effects of molybdenum and aluminum on the hot corrosion (sulfidation) behavior of experimental nickel-base superalloys [J]. Metallurgical and Materials Transactions B, 1972, 5(7): 673−683.
[9] LIU G M, ZHOU Y C，ZHANG Y M. Influence of pre-oxidation on the hot corrosion of Ti_3SiC_2 in the mixture of Na_2SO_4-NaCl melts [J]. Corrosion Science, 2006, 48, 650−661.
[10] YANG X, PENG X, WANG F. Hot corrosion of a novel electrodeposited Ni–6Cr–7Al nanocomposite under molten $(0.9Na, 0.1K)_2SO_4$ at 900 ℃ [J]. Scripta Materialia, 2007, 57: 891−894.
[11] GUPTA D K, RAPP R A. The solubilities of NiO, Co_3O_4 and ternary oxides in fused Na_2SO_4 at 1200 K [J]. Journal of the Electrochemical Society, 1980, 127: 2194−2202.
[12] ZHAO S Q, XIE X S, SMITH G D, PATEL S J. The corrosion of inconel alloy 740 in simulated environments for pulverized coal-fired boiler [J]. Materials Chemistry and Physics, 2005, 90: 275−281.
[13] RAPP P A, GOTO K S. Hot corrosion of metals by molten salts [C]//Second International Symposium on Molten Salts. Pennington. NJ: The Electrochemical Society, 1981: 81−82.
[14] SUSAN D R, MARDER A R. Ni-Al composite coatings: Diffusion analysis and coating lifetime estimation [J]. Acta Materialla, 2001, 49: 1153−1163.
[15] DAHL K V, HALD J, HORSEWELL A. Grey-scale conversation X-ray mapping by EDS of multielement and multiphase layered microstructures [J]. Journal of Microscopy, 2007, 225: 31−40.
[16] TOSHIO N, TAKESHI I, TAKUMI N, YOSHIMITSU S, KEMAS Z T, SHIGENARI H. Advanced coatings on high temperature applications [J]. Materials Science Forum, 2006, 522−523: 1−14.
[17] BRANDL W, MARGINEAN G, MARGINEAN N, CHIRILA V, UTU V. Prevention of metal dusting on Ni-based alloys by MCrAlY coatings [J]. Corrosion Science, 2007, 49(10): 3765−3771.
[18] SHEYBANY S, DOUGLASS D L. The effect of preoxidation on the corrosion of some superalloys in coal char [J]. Oxidation of Metals, 1988, 29 (3−4): 307−325.

Ni−16Cr−*x*Al 合金在 600 ℃ Na_2SO_4−NaCl 混合盐中的热腐蚀行为

李维杰[1], 刘 咏[1], 王 岩[1], 韩 朝[1], 汤慧萍[2]

1. 中南大学 粉末冶金国家重点实验室，长沙 410083；
2. 西北有色金属研究院 金属多孔材料国家重点实验室，西安 710016

摘 要：研究 Ni−16Cr−*x*Al(*x*=4.5%, 6.8%, 9.0%)合金在 600 ℃ Na_2SO_4−NaCl 混合盐中的热腐蚀行为，分析预氧化及铝含量对合金抗热腐蚀行为的影响。结果表明，随着铝含量由4.5%增加到9.0%(质量分数)，Ni−16Cr−*x*Al(*x*=4.5%, 6.8%, 9.0%)合金在 Na_2SO_4−NaCl 混合盐中的抗热腐蚀性能提高。因为 β-NiAl 相的存在能修复热腐蚀中被破坏的 Al_2O_3 膜，所以 Ni−16Cr−9.0Al 合金表现出最优异的抗热腐蚀性能。在预氧化后的样品表面形成了一层具有保护性的氧化膜，其抗热腐蚀性能优于原始态样品的。

关键词：Ni−16Cr−*x*Al 合金；预氧化；Na_2SO_4−25%NaCl 混合盐；热腐蚀机理

(Edited by LI Xiang-qun)